Journal of Fluids and Structures (1997) **11,** 327–344

FLUID TRANSPORT DUE TO NONLINEAR FLUID-STRUCTURE INTERACTION

J. S. JENSEN

Department of Solid Mechanics, Technical University of Denmark, DK-2800 Lyngby, Denmark

(Received 9 September 1996 and in revised form 15 December 1996)

This work considers nonlinear fluid–structure interaction for a vibrating pipe containing fluid. Transverse pipe vibrations will force the fluid to move relative to the pipe creating unidirectional fluid flow towards the pipe end. The fluid flow induced affects the damping and the stiffness of the pipe. The behavior of the system in response to lateral resonant base excitation is analysed numerically and by the use of a perturbation method (multiple scales). Exciting the pipe in the fundamental mode of vibration seems to be most effective for transferring energy from the shaker to the fluid, whereas higher modes of vibration can be used to transport fluid with pipe vibrations of smaller amplitude. The effect of the nonlinear geometrical terms is analysed and these terms are shown to affect the response for higher modes of vibration. Experimental investigations show good agreement with theoretical predictions.

1. INTRODUCTION

THIS WORK DEALS WITH FLUID FLOW in a vibrating pipe driven by nonlinear components of the vibratory forces. A theoretical and experimental investigation of system response to lateral resonant base excitation is carried out.

When a fluid-filled pipe performs transverse vibrations, transverse forces affect each fluid element. Depending on the pipe slope, components of the forces act tangentially to the pipe axis forcing the fluid element to move relative to the pipe. The bulk movement of the fluid is determined by the total contribution of tangential forces on all the fluid elements in the pipe. In the absence of external pressure forces, the axial motion of the fluid is governed completely by the nonlinear vibratory forces. In addition, the fluid motion induced nonlinearly affects the dynamic behavior of the pipe. Thus, the effect to be studied is governed by nonlinear interaction.

Previous work has been done on nonlinear dynamic interaction between structures and movable media in contact with the structure. Seemingly paradoxical behavior of vibrating rods with point-masses free to slide has been described by Blekhman & Malakhova (1986) and Chelomei (1983). Blekhman and Malakhova investigated systems of rigid and flexible rods, carrying collars with holes slightly larger than those of the rods. For certain conditions of excitation the rod could be stabilized in an upright position with a collar fixed in "flying" position along the rod. Linear theory predicts no coupling between collar- and rod-motion and the collar would be expected to simply fall under the influence of gravity. Also, the above-mentioned phenomenon is potentially applicable for passive vibration damping (Babitsky & Veprik 1993, Thomsen 1996).

Bajaj *et al.* (1980) and Rousselet & Herrmann (1981) considered nonlinear

0889–9746/97/030327 + 18 $25.00/fl960080

fluid–structure interaction in fluid-conveying pipes. The fluid was affected by a large upstream fluid pressure in addition to the weak nonlinear vibratory forces. Consequently, the effect of the nonlinear interaction forces was to modify the fluid speed on a small-scale level. Lee *et al.* (1995) investigated nonlinear interaction between longitudinal, transverse and radial vibrations of a pipe and the speed and pressure of conveyed fluid. In a case study, they considered a pinned–pinned pipe conveying fluid with prescribed speed.

Linear studies on structures traversed by moving point-masses have been studied by Sadiku & Leipholz (1987), for example. The point-mass speed was externally prescribed, and the effect of the moving mass on the structural behavior was analysed, while nonlinear interaction was neglected. Pipes conveying fluid have also been the subject of many investigations in the linear domain, [e.g. Benjamin (1961); Païdoussis & Issid (1974)]. These studies consider externally prescribed fluid speed, neglecting nonlinear interaction. For reviews of work on fluid-conveying pipes see, for example, Païdoussis & Li (1993) or Semler *et al.* (1994).

Also related to this work are studies on conveyance of solid material in vibrating rigid pipes or on plates. Long *et al.* (1994) investigated conveyance of a small solid block in a spatially curved tube by means of vibration. Sliding, non-sliding and flying motion of the block was considered. If careful attention was given to the excitation-amplitude and -frequency, the block could be transported through the tube. The motion of the rigid tube was prescribed and no attention was given to the influence of the motion of the block on the vibration of the tube. Other work on vibrational transportation of solid and granular material can be found in Blekhman (1994).

This paper is organized as follows. In Section 2 the model is presented and the equations of motion are derived. Section 3 presents numerically obtained solutions to the model equations. The results show that resonant pipe vibrations generally create unidirectional fluid flow towards the pipe end. In Section 4 a perturbation analysis is conducted (multiple scales). Results are presented for two specific examples: resonant excitation of the first and fourth mode of vibration, respectively. The effect of key parameters on system response is analysed, and so is the effect of the geometrical nonlinearities. The geometrical nonlinearities are shown to affect the response for higher modes of vibration. A comparison between the different modes of vibration with respect to energy transfer efficiency is provided, showing the fundamental mode to be most effective for transferring energy from the vibration exciter to the fluid. Section 5 describes experimental results for the first and second modes of vibration, showing good agreement with theoretically predicted results.

2. MODEL EQUATIONS

Figure 1(a) shows the model. A flexible cantilever pipe is connected to a fluid-filled reservoir, supplying fluid to the pipe. The fluid speed in the reservoir is vanishing, and the fluid pressure is atmospheric.

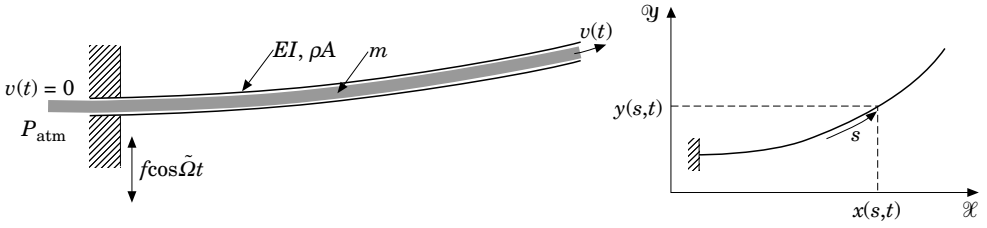

Figure 1. (a) System model, and (b) the coordinate system used.

The pipe is inextensible and uniform with length l, constant mass per length ρA, and flexural rigidity EI. The pipe performs in-plane transverse vibrations with small but finite rotations in the fixed coordinate system $(\mathscr{X}, \mathscr{Y})$, under the influence of lateral periodic base excitation given by the time-dependent displacement $f \cos \tilde{\Omega} t$. The pipe is slender, so that Bernoulli–Euler beam theory can be applied and rotary inertia be neglected. External dissipation is included in form of linear viscous damping.

The fluid is considered incompressible with mass per unit length m. The flow is described by the time-dependent speed $v(t)$. The fluid speed is taken as a mean of the cross-sectional speed profile and is measured positive towards the pipe end. The fluid flow is affected by internal friction between the fluid and the pipe wall, characterized by the pipe wall stress τ_{wall}.

Figure 1(b) shows the coordinate system. A pipe element is characterized by the position vector $\mathbf{r}(s, t) = (x(s, t), y(s, t))$, where $x(s, t)$ and $y(s, t)$ are the positions of the element along each axis in the fixed coordinate system $(\mathscr{X}, \mathscr{Y})$ respectively, and s is a curvilinear coordinate $s \in [0, l]$. The position of a fluid element relative to the pipe inlet is given by the curvilinear coordinate u, defined so that $\dot{u} = v$. The inextensibility condition provides the relation $(x')^2 + (y')^2 = 1$, where primes denote differentiation with respect to s.

Hamilton's principle is employed for setting up the equations of motion. The kinetic and potential energy density of a combined pipe- and fluid-element is, respectively:

$$\mathscr{T} = \tfrac{1}{2}\rho A \left|\frac{\partial \mathbf{r}}{\partial t}\right|^2 + \tfrac{1}{2} m \left|\frac{\mathrm{D}\mathbf{r}}{\mathrm{D}t}\right|^2 = \tfrac{1}{2}\rho A(\dot{y}^2 + \dot{x}^2) + \tfrac{1}{2} m(\dot{u}^2 + \dot{y}^2 + \dot{x}^2 + 2\dot{u}(\dot{y}y' + \dot{x}x')), \quad (1a)$$

$$\mathscr{V} = \tfrac{1}{2} EI\kappa^2 = \tfrac{1}{2} EI \frac{y''^2}{1 - y'^2}, \quad (1b)$$

where $\mathrm{D}/\mathrm{D}t \equiv \partial/\partial t + \dot{u}\,\partial/\partial t$. Dots denote differentiation with respect to time t.

The system Lagrangian $\mathscr{L}$ and the Lagrangian density $\mathscr{E}$ are introduced as

$$\mathscr{L} = \int_0^l (\mathscr{T} - \mathscr{V})\, \mathrm{d}s = \int_0^l \mathscr{E}\, \mathrm{d}s. \quad (2)$$

The variation of the action integral $I = \int_{t_1}^{t_2} \mathscr{L}\, \mathrm{d}t$ added to the virtual work done by the non-conservative forces acting on the system vanishes (Semler *et al.*, 1994),

$$\delta I + \int_{t_1}^{t_2} \delta \mathscr{W}\, \mathrm{d}t = 0. \quad (3)$$

The virtual work of nonconservative forces can be divided in two: $\delta \mathscr{W} = \delta \mathscr{W}_{\text{pipe}} + \delta \mathscr{W}_{\text{fluid}}$, i.e. the work associated with a virtual displacement of the pipe, and the work associated with a virtual displacement of the fluid. The two contributions are given as

$$\delta \mathscr{W}_{\text{pipe}} = -m\dot{u}\left(\frac{\partial \mathbf{r}_l}{\partial t} + \dot{u}\frac{\partial \mathbf{r}_l}{\partial s}\right) \cdot \delta \mathbf{r}_l = -m\dot{u}(\dot{y}_l \delta y_l + \dot{x}_l \delta x_l) - m\dot{u}^2(y_l' \delta y_l + x_l' \delta x_l), \quad (4a)$$

$$\delta \mathscr{W}_{\text{fluid}} = -\tau_{\text{wall}} l S_{\text{fluid}} \delta u + \frac{m}{\rho_{\text{fluid}}}(P_0 - P_l)\delta u. \quad (4b)$$

The virtual work done on the pipe (4a) equals the product of the virtual tip displacement and the fluid momentum. The virtual work on the fluid (4b) originates from the work done by the pipe-wall friction and by the difference in fluid pressure force between the pipe inlet and outlet, P_0 and P_l respectively, for a virtual displacement of a fluid element δu. In (4b), S_{fluid} and ρ_{fluid} denote the fluid tube circumference and the fluid density, respectively. External viscous damping is added later directly in modal form.

The last term in (4a) is rewritten using the inextensibility condition. The pipe-wall friction τ_{wall} of (4b) is proportional to the fluid speed for laminar flow, (White 1991), and to squared fluid speed for turbulent flow, (Bajaj *et al.* 1980). That is $\tau_{\text{wall}} = a_j \dot{u}\,|\dot{u}^{j-1}|$, where a_j is a pipe-wall friction coefficient, and $j = 1, 2$ for laminar and turbulent flow respectively. Assuming that the fluid discharges into atmospheric pressure, the Bernoulli equation (White 1991), can be used to relate the flow conditions at the pipe inlet to the conditions at the fluid reservoir. The fluid pressure difference can then be written as $P_0 - P_l = -\frac{1}{2}\rho_{\text{fluid}}\dot{u}^2$. Equations (4a,b) become

$$\delta \mathscr{W}_{\text{pipe}} = -m\dot{u}(\dot{y}_l \delta y_l + \dot{x}_l \delta x_l) - \int_0^l m\dot{u}^2 \Big(y''(1 + y'^2) - y'' \int_0^l y' y'' \, \mathrm{d}s \Big) \delta y \, \mathrm{d}s, \tag{5a}$$

$$\delta \mathscr{W}_{\text{fluid}} = -a_j l S_{\text{fluid}} \dot{u}\,|\dot{u}^{j-1}|\,\delta u - \tfrac{1}{2} m\dot{u}^2 \delta u. \tag{5b}$$

The variation of the action intgeral is

$$\delta I = \int_{t_1}^{t_2} \int_0^l \left(\frac{\partial \mathscr{E}}{\partial \dot{y}} \delta \dot{y} + \frac{\partial \mathscr{E}}{\partial y'} \delta y' + \frac{\partial \mathscr{E}}{\partial y''} \delta y'' + \frac{\partial \mathscr{E}}{\partial \dot{x}} \delta \dot{x} + \frac{\partial \mathscr{E}}{\partial x'} \delta x' + \frac{\partial \mathscr{E}}{\partial \dot{u}} \delta \dot{u} + \frac{\partial \mathscr{E}}{\partial u} \delta u \right) \mathrm{d}s \, \mathrm{d}t. \tag{6}$$

By using partial integration, eliminating x by using the inextensibility condition, and requiring (3) to be fulfilled for arbitrary admissible variations in δy and δu one obtains

$$\left(\frac{\partial}{\partial t} \frac{\partial \mathscr{E}}{\partial \dot{y}} + \frac{\partial}{\partial s} \frac{\partial \mathscr{E}}{\partial y'} - \frac{\partial^2}{\partial s^2} \frac{\partial \mathscr{E}}{\partial y''} \right) - y'(1 + \tfrac{1}{2} y'^2) \left(\frac{\partial}{\partial t} \frac{\partial \mathscr{E}}{\partial \dot{x}} + \frac{\partial}{\partial s} \frac{\partial \mathscr{E}}{\partial x'} \right)$$
$$+ y''(1 + \tfrac{3}{2} y'^2) \int_0^l \left(\frac{\partial}{\partial t} \frac{\partial \mathscr{E}}{\partial \dot{x}} + \frac{\partial}{\partial s} \frac{\partial \mathscr{E}}{\partial x'} \right) \mathrm{d}s + m\dot{u}^2 \Big(y''(1 + y'^2) - y'' \int_0^l y' y'' \, \mathrm{d}s \Big) = 0, \tag{7a}$$

$$\int_0^l \left(\frac{\partial}{\partial t} \frac{\partial \mathscr{E}}{\partial \dot{u}} - \frac{\partial \mathscr{E}}{\partial u} \right) \mathrm{d}s = -\tfrac{1}{2} m\dot{u}^2 - a_j l S_{\text{fluid}} \dot{u}\,|\dot{u}^{j-1}|. \tag{7b}$$

Equations (7a,b) are expanded, substituting $\dot{u} = v$. Small but finite pipe rotations imply that $(y')^2$ cannot be neglected compared to unity whereas $(y')^4$ and higher order terms can. This yields two coupled nondimensional equations governing the in-plane transverse vibrations of the pipe and the speed of the fluid, respectively:

$$\ddot{w} + w'''' + \left[w' \int_1^\xi \int_0^\xi (\dot{w}'^2 + w'\ddot{w}') \, \mathrm{d}\xi \, \mathrm{d}\xi \right]' + [w'[w'w'']']' + 2\beta U \dot{w}'(1 + w'^2)$$
$$+ U^2 w''(1 + w'^2) + \beta \dot{U}(1 - \xi) w''(1 + \tfrac{3}{2} w'^2) + w'' \int_1^\xi (2\beta U w'\dot{w}' + U^2 w' w''$$
$$+ \tfrac{1}{2}\beta \dot{U} w'^2) \, \mathrm{d}\xi = p\Omega^2 \cos \Omega\tau, \tag{8a}$$

$$\dot{U} + \frac{1}{\beta}(\alpha_j |U^{j-1}| + \tfrac{1}{2} U) U = -\beta \int_0^1 \left[\ddot{w} w' - (1 - \tfrac{1}{2} w'^2) \int_0^\xi (\ddot{w}' w' + \dot{w}'^2) \, \mathrm{d}\xi \right] \mathrm{d}\xi$$
$$+ \beta p \Omega^2 \sin \Omega\tau \int_0^1 w' \, \mathrm{d}\xi, \tag{8b}$$

valid for $\beta \neq 0$. Dots and primes here denote differentiation with respect to τ and ξ respectively, and the nondimensional quantities are:

$$\xi \equiv \frac{s}{l}, \qquad w \equiv \frac{y - f\cos\tilde{\Omega} t}{l}, \qquad p \equiv \frac{f}{l}, \qquad \tau \equiv \sqrt{\frac{EI}{(\rho A + m) l^4}}\, t, \qquad \Omega \equiv \sqrt{\frac{(\rho A + m) l^4}{EI}}\, \tilde{\Omega},$$
$$U \equiv \sqrt{\frac{ml^2}{EI}}\, v, \qquad \beta \equiv \sqrt{\frac{m}{\rho A + m}}, \qquad \alpha_1 \equiv \frac{a_1 S_{\text{fluid}} l^2}{\sqrt{mEI}}, \qquad \alpha_2 \equiv \frac{a_2 S_{\text{fluid}} l}{m}. \tag{9}$$

The first and second term in (8a) represents linear and stiffness respectively and the third and fourth term the nonlinear inertia and stiffness. The remaining terms on the left-hand side represent the fluid effect on the pipe vibrations due to the Coriolis, centrifugal and angle-acceleration forces. Equation (8a) is similar to equations previously obtained [e.g., Semler *et al.* (1994)] except for the presence of the external forcing term.

The left-hand side of the fluid equation (8b) contains the inertia and friction terms. The right-hand side describes the vibratory forcing from the transverse pipe motion. The equation agrees with those of Bajaj *et al.* (1980) and Rousselet & Herrmann (1981), except that there is no upstream fluid pressure in (8b). Hence, in the system considered fluid motion occurs only through coupling to the transverse pipe motion.

A mode-shape expansion is applied in order to recast equation (8a,b) into a set of ordinary differential equations. Using the expansion $w(\xi, \tau) = \sum_{i=1}^{n} q_i(\tau)\varphi_i(\xi)$, where $\varphi_i(\xi)$ is the orthogonal set of cantilever mode shapes, and $q_i(\tau)$ are the generalized coordinates, yields n ordinary differential equations for the pipe and a single ordinary equation for the fluid:

$$\ddot{q}_i + 2\zeta_i\omega_i\dot{q}_i + \omega_i^2 q_i + 2\beta U \sum_{k=1}^{n} k_{ik}\dot{q}_k + \sum_{k=1}^{n} (\beta f_{ik}\dot{U} + g_{ik}U^2)q_k + 2\beta U \sum_{k,l,m=1}^{n} K_{iklm}q_k q_l \dot{q}_m$$

$$+ \sum_{k,l,m=1}^{n} (\Lambda_{iklm} + \tfrac{1}{2}\beta F_{iklm}\dot{U} + G_{iklm}U^2)q_k q_l q_m + \sum_{k,l,m=1}^{n} \chi_{iklm}q_k(q_l\ddot{q}_m + \dot{q}_l\dot{q}_m)$$

$$= p\vartheta_i\Omega^2 \cos\Omega\tau, \quad \text{for } i = 1, \ldots, n, \quad (10a)$$

$$\dot{U} + \frac{1}{\beta}(\alpha_j |U^{j-1}| + \tfrac{1}{2}U)U = -\beta \sum_{k,l=1}^{n} k_{kl}q_k\ddot{q}_l - \beta \sum_{k,l=1}^{n} h_{kl}(q_k\ddot{q}_l + \dot{q}_k\dot{q}_l)$$

$$- \tfrac{1}{2}\beta \sum_{k,l,m,p=1}^{n} H_{klmp}q_k q_l(q_m\ddot{q}_p + \dot{q}_m\dot{q}_p). \quad (10b)$$

In equation (10a) modal viscous damping, characterized by the modal damping ratio ζ_i, has been added. In (10b) the explicit dependence on the base excitation has been neglected, since the base displacement amplitude is assumed to be much smaller than the pipe deflection ($p \ll q$). The constants: ω_i, ϑ_i, k_{ik}, g_{ik}, h_{ik}, Λ_{iklm}, F_{iklm}, G_{iklm}, χ_{iklm} and H_{klmp} are computed from the expansion functions (see Appendix).

If the forcing frequency Ω is near a natural frequency ω_i, then a single cantilever mode shape will be dominant and a single-mode approximation ($n = 1$) can be applied. Since the near-resonant case yields the largest pipe motion and thus the strongest vibratory forcing of the fluid, this case is of interest and will be considered in the following.

3. NUMERICAL ANALYSIS OF SYSTEM BEHAVIOR

In this section time-series are shown depicting the basic fluid and pipe motion. As examples, results are given for the first and fourth modes of vibration for excitation in sharp resonance, i.e. $\Omega = \omega_i$, $i = 1, 4$. The results are based on numerical integration (fifth- and sixth-order runge-Kutta-Verner) of the single-mode approximation of equations (10a,b), written as a system of three first order equations.

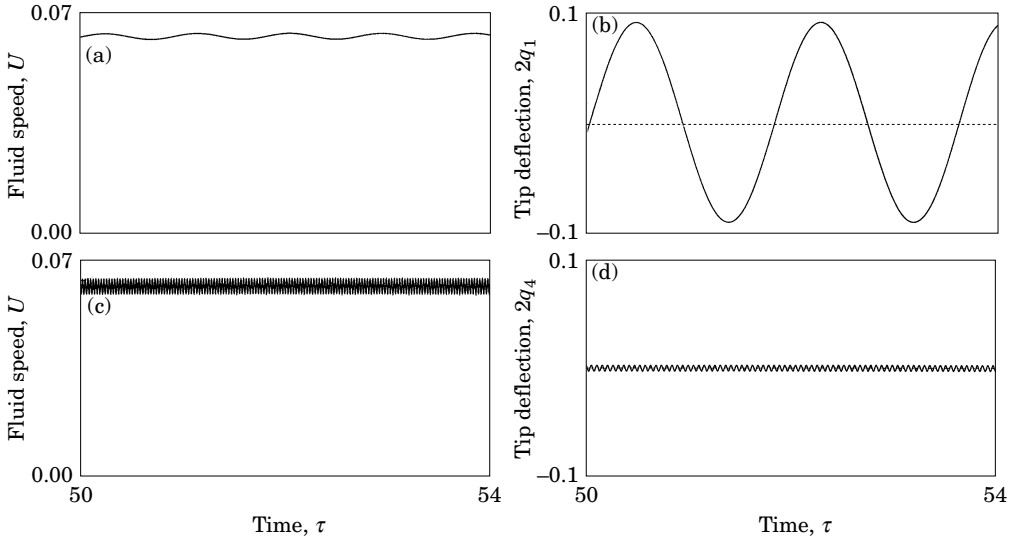

Figure 2. Numerical simulation of system behavior for the first and the fourth modes of vibration: (a,c) fluid speed U, and (b,d) pipe end deflection $2q_i$; (a,b) $\Omega = \omega_1$, $p = 0{\cdot}003$; (c,d) $\Omega = \omega_4$, $p = 0{\cdot}00015$; $\alpha_2 = 0{\cdot}8$; in all cases, $j = 2$, $\alpha_2 = 0{\cdot}8$, $\beta^2 = 0{\cdot}2$, $\zeta = 0{\cdot}01$.

Figure 2(a,c) depicts the fluid speed as a function of time for the first and fourth mode of vibration, respectively. A positive mean fluid speed appears, indicating flow in the direction towards the pipe end. Small oscillations are seen to overlay the mean speed. The amplitude and frequency of the oscillations increase with the mode number, but the amplitude is always small compared to the mean speed. Figure 2(b,d) shows the corresponding deflections of the pipe end. The vibrations are seen to be regular periodic, with maximum tip deflection around 9% of the pipe length for vibrations in the first mode and around 0·3% for the fourth mode. The significant difference in vibration amplitude is seen even though the corresponding values of the mean fluid speed are comparable.

It should be emphasized that even though the mean fluid speed, when exciting the fourth mode of vibration with very little amplitude of excitation, is comparable to the mean fluid speed with first mode excitation at considerable higher magnitudes, this is not a good base of comparison between the two modes of vibration. As will appear later, from Section 4.3, the fourth-mode excitation represents a higher power consumption, due to the difference in natural frequencies between the two modes.

According to the model, mean flow is shown to be induced in the pipe, when the pipe vibrates. Similar qualitative behavior as in Figure 2 is seen for a wide range of parameters in the case of near-resonant forcing. It can be shown also that all modes of vibration create the displayed effect. The shown effect is purely nonlinear and is to be analysed in further detail in the following sections.

4. PERTURBATION ANALYSIS OF RESONANT MOTION

A perturbation analysis of the model equations is performed in order to obtain more insight into the behavior of the system, and to analyse the effect of variation of the system parameters. A multiple scales method [e.g., Nayfeh & Mook (1979)] is employed for obtaining results for the near-resonant case. Only positive values of the fluid speed are considered, i.e. $|U^{j-1}| = U^{j-1}$.

To perform the analysis, two different time-scales are introduced. A fast time-scale T_0 comparable with natural- and excitation-frequencies, and a slow time-scale $T_1 = \varepsilon T_0$ describing the slow modulation of the pipe-amplitude and -phase and of the mean fluid speed. The small parameter ε is introduced in order to indicate small terms.

Analysing the system response in the near resonant case, a single-mode approximation of equations (10a,b) is applied:

$$\ddot{q}_i + \omega_i^2 q_i + 2\varepsilon(\zeta_i\omega_i + \beta k_{ii}U)\dot{q}_i + \varepsilon(\beta f_{ii}\dot{U} + g_{ii}U^2)q_i + \varepsilon(\Lambda_{iiii} + \tfrac{1}{2}\beta F_{iiii}\dot{U} + G_{iiii}U^2)q_i^3 + 2\varepsilon\beta U K_{iiii}q_i^2\dot{q}_i + \varepsilon\chi_{iiii}q_i(q_i\ddot{q}_i + \dot{q}_i^2) = \varepsilon p\vartheta_i\Omega^2\cos\Omega\tau, \quad (11a)$$

$$\dot{U} + \frac{\varepsilon}{\beta}(\alpha_j U^{j-1} + \tfrac{1}{2}U)U = -\varepsilon\beta k_{ii}q_i\ddot{q}_i - \varepsilon\beta(h_{ii} + \tfrac{1}{2}H_{iiii}q_i^2)(q_i\ddot{q}_i + \dot{q}_i^2). \quad (11b)$$

In (11a) and (11b), nonlinear terms, damping terms and forcing terms have been considered to be of order ε compared to inertia terms, respectively. In the following, indices indicating the mode number are omitted for brevity.

A zero-order approximation to equations (11) is sought. To obtain this, a first-order expansion is introduced,

$$q = q_0(T_0, T_1) + \varepsilon q_1(T_0, T_1), \qquad U = U_0(T_0, T_1) + \varepsilon U_1(T_0, T_1). \quad (12a,b)$$

Inserting (12a,b) into (11a,b) and equating coefficients of the same powers in ε, yields to order ε^0:

$$D_0^2 q_0 + \omega^2 q_0 = 0, \qquad D_0 U_0 = 0; \quad (13a,b)$$

and to order ε^1:

$$D_0^2 q_1 + \omega^2 q_1 = -2D_0D_1q_0 - 2(\zeta\omega + \beta kU_0)D_0q_0 - (\beta f D_0U_0 + gU_0^2)q_0 - (\Lambda + \tfrac{1}{2}\beta F D_0U_0 + GU_0^2)q_0^3 - 2\beta K U_0 q_0^2 D_0q_0 - \chi q_0(q_0D_0^2q_0 + (D_0q_0)^2) + \rho\vartheta\Omega^2\cos\Omega\tau, \quad (14a)$$

$$D_0U_1 = -D_1U_0 - \frac{1}{\beta}(\alpha_j U_0^{j-1} + \tfrac{1}{2}U_0)U_0 - \beta k q_0 D_0^2 q_0 - \beta(h + \tfrac{1}{2}Hq_0^2)(q_0D_0^2q_0 + (D_0q_0)^2), \quad (14b)$$

where $D_j^i \equiv \partial^i/\partial T_j^i$.

The solutions to (13a,b) are

$$q_0 = B e^{i\omega T_0} + \bar{B}e^{-i\omega T_0}, \qquad U_0 = A, \quad (15a,b)$$

where A and B are real and complex functions of T_1, respectively. A bar denotes the complex conjugate.

The unknown functions A and B are to be determined. Substituting (15a,b) into the ε^1-order equations (14a,b), yields

$$D_0^2 q_1 + \omega^2 q_1 = -(2i\omega B' + 2i\omega(\zeta\omega + \beta kA)B + gA^2B)e^{i\omega T_0} - (3\Lambda + 3GA^2 + 2i\omega\beta KA - 2\omega^2\chi)B^2\bar{B}e^{i\omega T_0} - (\Lambda + GA^2 + 2i\omega\beta KA - 2\omega^2\chi)B^3e^{3i\omega T_0} + \tfrac{1}{2}p\vartheta\Omega^2 e^{i\Omega T_0} + \text{cc}, \quad (16a)$$

$$D_0U_1 = -\tfrac{1}{2}A' - \frac{1}{2\beta}(\alpha_j A^{j-1} + \tfrac{1}{2}A)A + \beta\omega^2(k + HB\bar{B})B\bar{B} + \beta\omega^2(k + 2h + 2HB\bar{B})B^2e^{2i\omega T_0} + \beta\omega^2 HB^4e^{4i\omega T_0} + \text{cc}, \quad (16b)$$

where $(\ )' = \partial/\partial T_1$, and cc denotes the complex conjugates of the preceding terms.

Terms proportional to $e^{i\omega T_0}$ and terms independent of T_0 yield secular terms in the solution to (16a) and (16b), respectively. The case of $\Omega \approx \omega$ yields a near-resonant term in (16a), which will produce a small divisor term in the solution. These terms are required to vanish.

The nearness of the excitation frequency to the natural frequencies can be expressed as

$$\Omega = \omega + \varepsilon\sigma \Leftrightarrow \Omega T_0 = \omega T_0 + \sigma T_1, \tag{17}$$

where σ is a so-called detuning parameter. Inserting (17) into (16a,b) and eliminating the resonant and near resonant terms in (16a) and constant terms in (16b) yields, upon separating real and imaginary part for the pipe equation,

$$\omega b' = -\omega(\zeta\omega + \beta k A)b - \tfrac{1}{4}\beta\omega K A b^3 + \tfrac{1}{2}p\vartheta\Omega^2 \sin\psi, \tag{18a}$$

$$\omega b\psi' = (\omega\sigma - \tfrac{1}{2}gA^2)b - \tfrac{3}{8}(\Lambda + GA^2 - \tfrac{2}{3}\omega^2\chi)b^3 + \tfrac{1}{2}p\vartheta\Omega^2 \cos\psi, \tag{18b}$$

$$\beta A' = -(\alpha_j A^{j-1} + \tfrac{1}{2}A)A + \tfrac{1}{2}\beta^2\omega^2(k + \tfrac{1}{4}Hb^2)b^2, \tag{18c}$$

where the polar notation $B \equiv \frac{1}{2}b e^{i(\sigma T_1 - \psi)}$, b and ψ being real functions of T_1, has been introduced.

Equations (18a–c) constitute the so-called modulation equations, i.e. they govern the slow time-scale modulation of the pipe-amplitude and -phase, b and ψ, and of the mean fluid speed, A.

4.1. First Vibration Mode, Linear Geometry

The system is considered for $i = 1$, i.e. the forcing frequency is chosen near the fundamental natural frequency ($\Omega = \omega_1$), so that the fundamental mode of vibration is dominant.

The stationary behavior of the system is obtained by setting $b' = \psi' = A' = 0$ in (18a,c). For low-to-moderate amplitude of forcing ($p \lesssim 0{\cdot}2$), the effect of the higher order geometrical nonlinearities is inessential. Neglecting these higher-order terms, the stationary solution for the modal pipe amplitude b_1 and the mean fluid speed A become

$$\tfrac{1}{4}p^2\vartheta_1^2\Omega^4 = [\omega_1^2(\zeta_1\omega_1 + \beta k_{11}A)^2 + (\tfrac{1}{2}g_{11}A^2 - \omega_1(\Omega - \omega_1))^2]b_1^2, \tag{19a}$$

$$(\alpha_j A^{j-1} + \tfrac{1}{2}A)A = \tfrac{1}{2}\beta^2\omega_1^2 k_{11} b_1^2. \tag{19b}$$

Equation (19b) is used to eliminate A from (19a). Equation (19a) is then solved for b_1 using a Newton-Raphson method. The stability of the solutions is determined by computing the eigenvalues of the Jacobian of (18a,b), evaluated at the solution points.

Figure 3 shows frequency response curves depicting the mean fluid speed A and the tip amplitude $2b_1$ versus the relative forcing frequency $\Omega\omega_1$. The perturbation solution, based on (19a,b), is compared to results obtained by numerical integration of (11a,b) without the geometrical nonlinearities. The tip amplitude is also compared to the linear case with the fluid fixed inside the pipe, corresponding to setting $A = 0$ in (19a).

As appears from Figure 3(b), significant motion of the pipe is confined to a frequency band near the linear resonance frequency $\Omega = \omega_1$. This is reflected in the fluid behavior, shown in Figure 3(a) in that, outside the resonant region, the vibrations

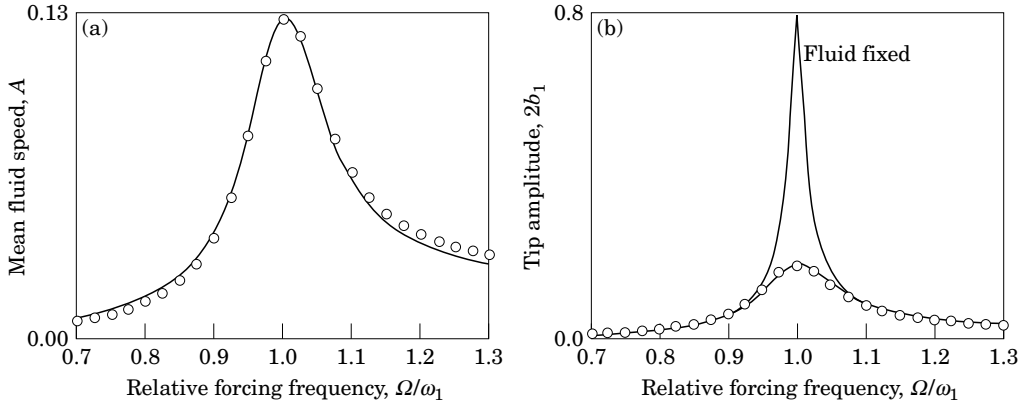

Figure 3. (a) Mean fluid speed A and (b) tip amplitude $2b_1$ for the fundamental mode of vibration ($i = 1$), versus relative forcing frequency Ω/ω_1 for $p = 0{\cdot}01$: ——, stable solutions; ○, numerical integration; $j = 2$, $\alpha = 0{\cdot}8$, $\beta^2 = 0{\cdot}2$, $\zeta_1 = 0{\cdot}01$.

of the pipe are too small to induce significant fluid motion. The nonlinear coupling to the fluid damps the vibrations of the pipe in the resonant region, as appears from Figure 3(b). Compared to the case where the fluid is fixed inside the pipe, the amplitude of the pipe vibrations is reduced significantly, due to large energy transfer to the fluid (see also Section 4.3). The fluid flow also slightly increases the stiffness of the pipe. This appears as a slight bending to the right of the response curves (hardly noticeable in the figure). For other modes of vibration, the fluid flow has a softening effect, bending response curves to the left. In all cases this effect is small compared to the effect of damping. From comparison with numerical results it appears that the perturbation solution adequately describes the qualitative behavior of the system.

Figure 4 shows the effect of four key system parameters on the mean fluid speed A: forcing amplitude p, mass ratio β^2, turbulent wall friction coefficient α_2 and modal viscous damping ratio ζ_1. The response is shown in a forcing frequency domain near the linear resonance frequency $\Omega = \omega_1$.

Figure 4(a,b) shows the effect of the amplitude of base excitation and the amount of viscous damping. The values of these parameters directly influence the amplitude of the pipe vibrations, but only indirectly influence the fluid speed. Increasing p or decreasing ζ_1 results in larger amplitude of vibrations, which increases the fluid speed. If the viscous damping is increased, the response curves are also seen to flatten.

Figure 4(c,d) depicts the effect of the relative fluid mass and the turbulent wall-friction coefficient. Both parameters directly influence the mean fluid speed. Increasing α_2 restricts fluid flow and decreasing β^2 decreases the magnitude of the nonlinear pipe–fluid coupling. In both cases the mean fluid speed is decreased. Decreased mean speed lowers the fluid damping on the pipe vibrations, and lower mass ratio will also directly reduce the fluid effect on the pipe motion. Consequently, the amplitude of pipe vibrations will grow. This will affect the fluid, but this secondary effect is small compared to the direct influence.

Two limit curves are shown. The case of $\beta^2 = 1$ in Figure 4(c) represents the maximum nonlinear coupling, i.e. a dense fluid in a thin-walled pipe of light material. Maximum nonlinear coupling maximizes A, i.e. the nondimensional mean fluid speed. Large nonlinear coupling also maximizes the damping of the pipe vibrations, resulting in a smooth response curve. The limit case of $\alpha_2 = 0$ in Figure 4(d) maximizes the mean fluid speed, since the fluid then flows freely through the pipe. The flow is, however,

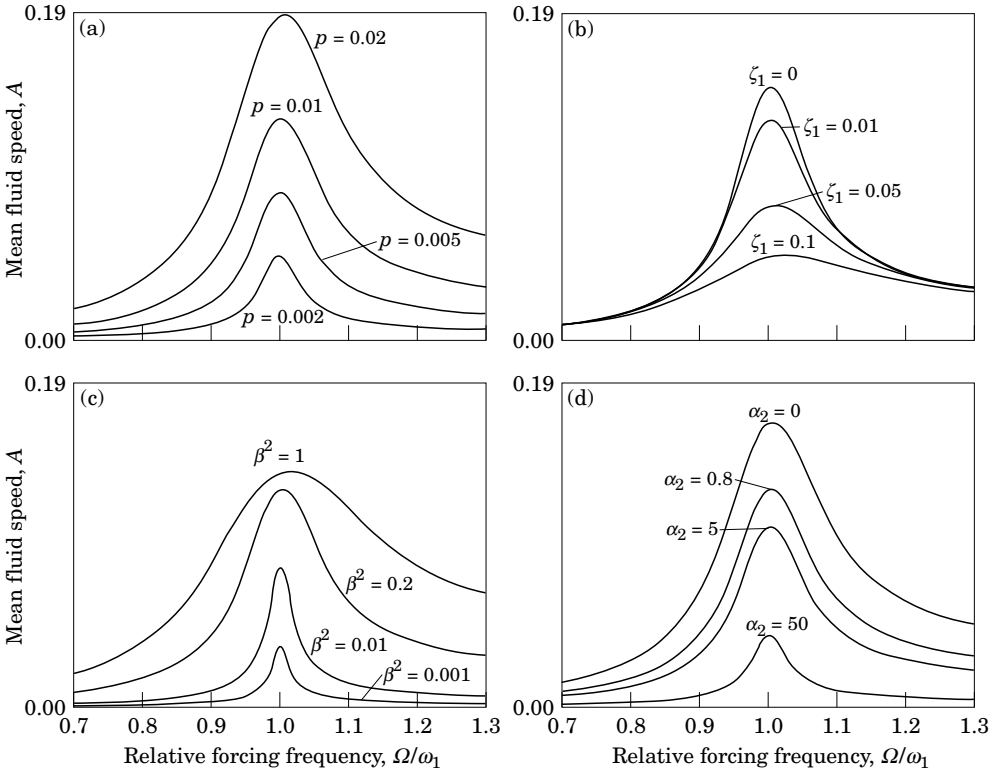

Figure 4. Mean fluid speed A versus relative forcing frequency Ω/ω_1, showing (a) effect of forcing amplitude p, (b) effect of mass ratio β^2, (c) effect of turbulent coefficient α_2 and (d) effect of external viscous modal damping coefficient ζ_1; parameter values are (unless explicitly stated): $p = 0{\cdot}01$, $\alpha_2 = 0{\cdot}8$, $\beta^2 = 0{\cdot}2$, $\zeta_1 = 0{\cdot}01$.

still restricted, due to the stationary fluid in the upstream fluid reservoir which has to be accelerated.

4.2. Fourth Vibration Mode, Nonlinear Geometry

The forcing frequency is now assumed to be near the fourth natural frequency ($i = 4$, $\Omega \approx \omega_4$), so that the fourth mode of vibration is dominant. The third-order geometrical nonlinearities will qualitatively affect the system response even for low-amplitude excitation of the base. Including these higher-order geometrical nonlinearities, the stationary solution to (18a,c) can be found to be

$$\tfrac{1}{4}p^2\vartheta_4^2\Omega^4 = [[(\tfrac{1}{2}g_{44}A^2 - \omega_4(\Omega - \omega_4)) + \tfrac{3}{8}(\Lambda_{4444} + G_{4444}A^2 - \tfrac{2}{3}\omega_4^2\chi_{4444})b_4^2]^2 + [\omega_4(\zeta_4\omega_4 + \beta k_{44}A) + \tfrac{1}{4}\beta\omega_4 K_{4444}Ab_4^2]^2]b_4^2, \tag{20a}$$

$$(\alpha_j A^{j-1} + \tfrac{1}{2}A)A = \tfrac{1}{2}\beta^2\omega_4^2(k_{44} + \tfrac{1}{4}H_{4444}b_4^2)b_4^2. \tag{20b}$$

Figure 5 shows frequency response curves depicting the mean fluid speed A and the tip amplitude $2b_4$ versus the relative forcing frequency $\Omega\omega_4$. The perturbation solution, based on (20a,b), is compared to results obtained by numerical integration of

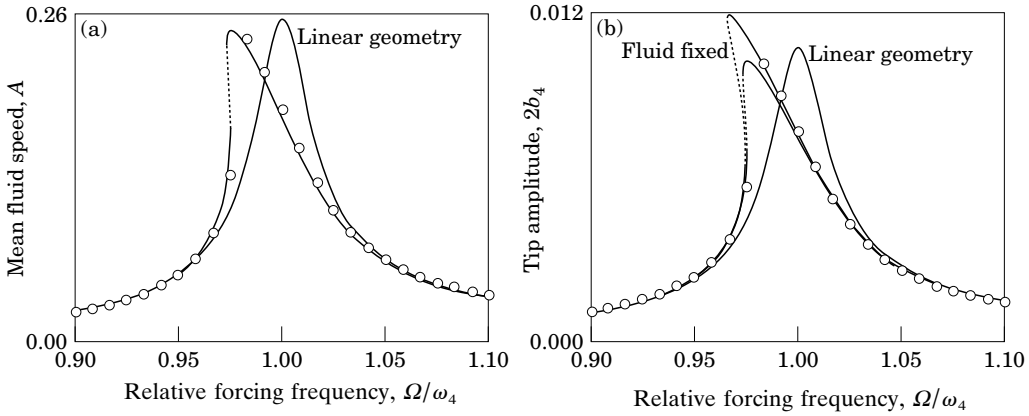

Figure 5. (a) Mean fluid speed A and (b) pipe end amplitude $2b_4$ for the fourth vibration mode ($i = 4$), versus relative forcing frequency Ω/ω_4 for $p = 0{\cdot}0007$: ——, · · ·, stable, unstable solutions; ○, numerical integration: $j = 2$, $\alpha_2 = 0{\cdot}8$, $\beta^2 = 0{\cdot}2$, $\zeta_4 = 0{\cdot}01$.

a single mode approximation of (11a,b). The tip amplitude is also compared to the case of a fixed fluid, corresponding to letting $A = 0$ in (20a), and to the case where the higher order geometrical nonlinearities are neglected in (20a,b).

Figure 5(b) indicates how the nonlinear geometrical terms affect the system response. A left-bending of the frequency response curve appears. This effect is due to nonlinear inertia which has a softening effect. Nonlinear inertia is the dominant third-order geometrical nonlinearity for second and higher modes of vibration. For the fundamental mode, nonlinear curvature is dominant, pulling the response curves slightly to the right. This effect is, however, negligible as mentioned in Section 4.1. Figure 5(b) shows that the damping effect of the fluid on the vibrations of the pipe is much less prominent compared to vibrations in the first mode, due to less transfer of energy to the fluid. The response curve is seen to match the case of a fixed fluid nearly if the relative frequency of forcing Ω/ω_4 is increased slowly (the response jumps to the upper stable solution branch at $\Omega \approx 0{\cdot}975$). If, however, Ω/ω_4 is decreased slowly past the resonance region the response is ''topped off'' due to the nonlinear coupling to the fluid. At the linear resonance frequency, the pipe amplitude nearly matches the response with the fluid being fixed.

Figure 5(a) shows response curves for the mean fluid speed A. The left bending of the response curve reduces A by approximately 25% at the linear resonance frequency, compared to the case where the third-order geometrical nonlinearities are neglected. The maximum attainable fluid speed is, however, almost unchanged, but depends on if the forcing frequency is increased or decreased through the resonant region.

Figure 6 displays the effect of four key system parameters on the mean fluid speed A: forcing amplitude p, mass ratio β^2, turbulent wall friction coefficient α_2 and modal viscous damping ζ_4.

Figure 6(a,b) shows the effect of p and ζ_4. Changing the amplitude of forcing and the amount of modal viscous damping affects the amplitude of vibrations directly. Larger forcing and weaker damping increase the amplitude, causing the geometrical nonlinearities to come into effect. This is directly reflected in the fluid response curves, bending them to the left. The amount of viscous damping is critical, as appears from Figure 6(b). If the damping ratio exceeds about 5%, the resonant top vanishes with low mean fluid speed as a result.

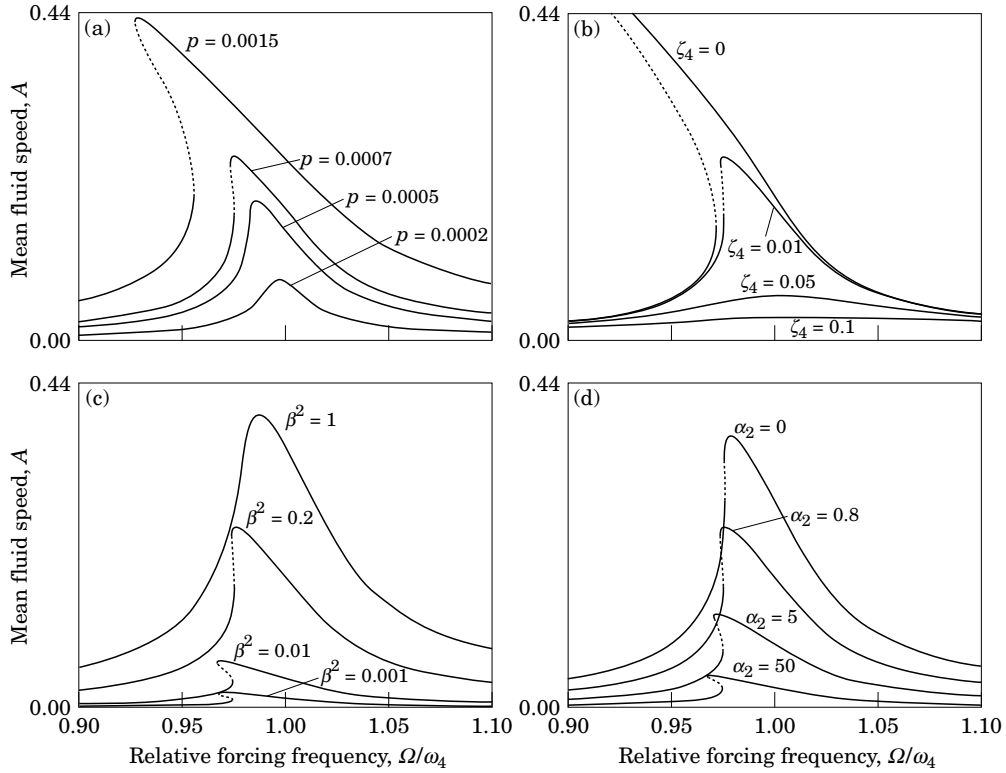

Figure 6. Mean fluid speed A versus relative forcing frequency Ω/ω_4, showing (a) effect of forcing amplitude p, (b) effect of mass ratio β^2, (c) effect of turbulent friction coefficient α_2 and (d) effect of external viscous modal damping coefficient ζ_4; ——, · · ·; Stable, unstable solutions; parameter values (unless explicicly stated in the figures): $p = 0{\cdot}0007$, $j = 2$, $\alpha_2 = 0{\cdot}8$, $\beta^2 = 0{\cdot}2$, $\zeta_4 = 0{\cdot}01$.

Figure 6(c,d) shows the effect of the mass ratio β^2 and the turbulent wall friction α_2. Changing these parameters affects the fluid speed directly. Increasing the amount of wall friction increases the resistance on the fluid flow; similarly, decreasing the mass ratio decreases the nonlinear pipe–fluid coupling. The secondary effect on the fluid, mentioned in Section 4.1, is noticeable here. With decreased mean fluid speed, the fluid damping of the pipe vibrations is decreased, which causes the geometrical nonlinearities to come into effect. This is reflected in the fluid response curves, causing bending to the left.

4.3. Energy Transfer Considerations

In this section the energy transfer mechanism in the system is analysed. By means of nonlinear interaction, energy is transferred from the vibration exciter to the fluid, resulting in nonzero mean fluid speed and damped pipe vibrations. An account for this mechanism is made from the numerical solution of the single-mode approximation of equations (10a,b), with the higher order geometrical nonlinearities neglected. If both sides of equation (10a) are multiplied with the modal pipe velocity $\dot{q}$, the equation then expresses a dimensionless power balance for the system. The left-hand side of the equation expresses the kinetic and elastic power in the pipe, as well as the dissipated power and the kinetic power in the fluid. The right-hand side is a measure of the instantaneous power supplied by the shaker. If both sides of the equation are

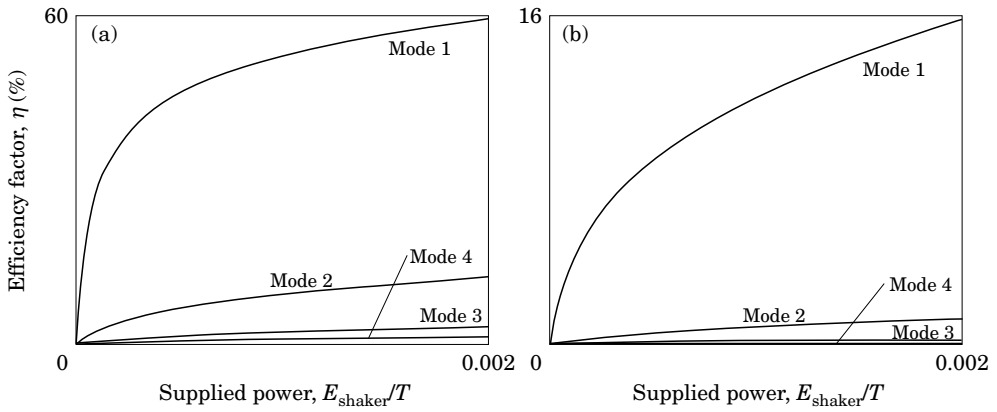

Figure 7. Efficiency factor η versus supplied power E_{shaker}/T, (a) for $\zeta_i = 0{\cdot}01$, and (b) for $\zeta_i = 0{\cdot}05$, for the four lowest modes of vibration; $\Omega = \omega_i$, $j = 2$, $\alpha_2 = 0{\cdot}8$, $\beta^2 = 0{\cdot}2$.

integrated over a single forcing period $T = 2\pi/\Omega$, a dimensionless energy balance is obtained. The kinetic and elastic energies of the pipe vanish when integrated over a forcing period. Consequently, the energy supplied is either dissipated or transformed into kinetic energy of the fluid.

An efficiency factor for the shaker/fluid energy transfer mechanism, η, is then defined as follows:

$$\eta \equiv \frac{E_{\text{fluid}}}{E_{\text{shaker}}} = \frac{\displaystyle\int_0^{2\pi/\Omega} \dot{q}_1(2\beta k_{ii} U \dot{q}_i + \beta f_{ii} \dot{U} q_i + g_{ii} U^2 q_i)\, \mathrm{d}\tau}{\displaystyle\int_0^{2\pi/\Omega} \dot{q}_i p \vartheta_i \Omega^2 \cos \Omega\tau \, \mathrm{d}\tau}, \tag{21}$$

where E_{shaker} and E_{fluid} are nondimensional measures of the supplied energy from the shaker and the kinetic energy of the fluid, respectively. Using (21) with (10a,b), the efficiency factor can be computed for different modes of vibration and parameters.

Figure 7 shows the efficiency factor η for the four lowest modes of vibration as a function of the nondimensional power E_{shaker}/T, supplied by the shaker, for two different values of the modal damping ratio ζ_i. The modal damping ratio is in both cases assumed to be identical for the four modes considered.

It appears that the fundamental mode of vibration is the most effective for transferring energy from the shaker to the fluid. It is noted also that η drops significantly for higher modes of vibration. The efficiency factor is seen to increase for higher power input, but the increase drops off quickly with increased power. For all modes of vibration the efficiency factor depends strongly on the amount of viscous damping present in the system. Comparing Figure 7(a) and 7(b), larger damping is seen to cause less efficient transport of fluid, due to a larger dissipation of energy.

5. EXPERIMENTAL INVESTIGATION

Experiments were carried out for horizontal acrylic pipes subjected to resonant excitation. Two different pipes were used to investigate fluid motion in response to first- and second-mode vibrations. The experiments are set to cover both laminar and turbulent flow for both modes considered.

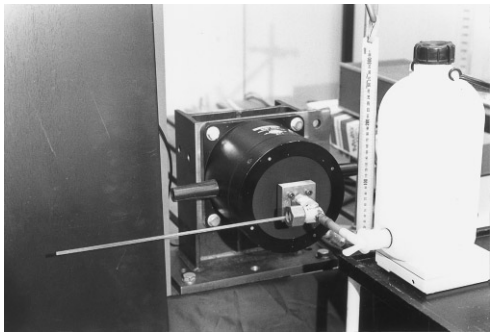

(a)

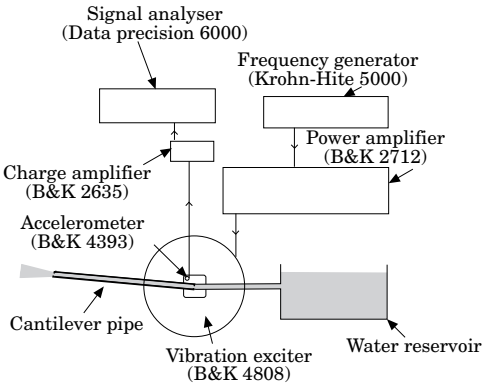

(b)

Figure 8. (a) Experimental set-up and (b) schematic of the set-up.

5.1. Experimental Set-up

Figure 8 shows the experimental set-up. The pipe is mounted on a shaker with a steel socket, and acrylic fittings are used to tighten the pipe. Water is allowed to flow in the pipe from a reservoir, through a short silicone rubber tube. The reservoir is placed on weighting scales, enabling the mass of the reservoir to be determined. A power amplifier feeds the shaker. The frequency and magnitude of the harmonic base displacement can be adjusted on the frequency generator connected to the power amplifier. The acceleration of the base is measured by an accelerometer mounted on the moving part of the shaker. The signal from the accelerometer is led through a charge amplifier to the signal analyser.

In order to be able to perform the experiments, the pipes have to be inclined slightly. Otherwise fluid will inevitably discharge from the pipe, even for a nonvibrating pipe. The inclination causes gravity forces to come into effect and restrict the fluid flow. This is counteracted in the experiments by increasing the water level in the reservoir so it matches the level of the pipe end.

The experimental procedure was as follows. The reservoir is filled so that the pipe is completely full of water. The natural frequency of the filled pipe is determined by slowly sweeping the excitation frequency and noting the frequency for maximum tip deflection. After refilling the reservoir, the mass of the reservoir is noted. The pipe is then forced with a frequency matching the natural frequency, and current power is adjusted to match the desired amplitude of forcing. After a forcing period of 20–120 s, depending on the actual fluid speed, the mass of the reservoir is noted again, so the amount of discharged fluid can be computed.

5.2. Material Data

Table 1 lists the data of the two pipes and water.

Young's modulus E is found by measuring the damped natural frequencies for the empty pipes and correcting for damping. A common mean value for the two pipes has been chosen. The friction coefficients α_1, α_2 are determined by measuring the volume flow in a nonvibrating pipe. The volume flow is created by applying a constant gauge-pressure in the reservoir. Adding this constant pressure term to the right-hand side of equation (8b), and with vanishing vibratory forcing, the equation can be solved for α_i, $i = 1, 2$. The viscous damping coefficient ζ has been computed by measuring the

TABLE 1
Material data for the two pipes

Pipe	1	2
Length, l (m)	0·40	0·60
Inner diameter, D_i (m)	$4{\cdot}70 \times 10^{-3}$	$4{\cdot}80 \times 10^{-3}$
Outer diameter, D_o (m)	$7{\cdot}10 \times 10^{-3}$	$7{\cdot}25 \times 10^{-3}$
Young's modulus, E (N/m^3)	$2{\cdot}15 \times 10^{9}$	$2{\cdot}15 \times 10^{9}$
Pipe density, ρ_{pipe} (kg/m^3)	$1{\cdot}24 \times 10^{3}$	$1{\cdot}24 \times 10^{3}$
Fluid density, ρ_{fluid} (kg/m^3)	998	998
Mass ratio, β^2	0·39	0·39
Laminar friction coefficient, α_1	0·10	0·22
Turbulent friction coefficient, α_2	2·6	3·9
Viscous damping coefficient, ζ_i	0·04	0·03

vibration amplitude for resonant vibrations of an empty pipe, and using standard results for a linear oscillator.

5.3. EXPERIMENTAL RESULTS

Experimental results for the two pipes are shown and compared with theoretical results. The theoretical results are based on the perturbation solution in equations (19a,b), i.e. the model with linear geometry. For the given parameter values the third-order geometrical nonlinearities have no influence on the response. The volume flow, V, is chosen as base of comparison between the analytical and the experimental results.

Figure 9 shows theoretical and experimental values for V, versus the excitation amplitude p for pipes 1 and 2. The volume flow is measured in milliliters per second [ml/s].

A laminar and a turbulent theoretical curve is shown for both pipes. The Reynolds number at the crossing of the two curves are computed to 2250–2300 for both pipes. This matches the theoretical values for pipe flow: 2000–2300, (White 1991). Thus the experimentally determined values for external damping and pipe-wall friction can be expected to be adequately accurate.

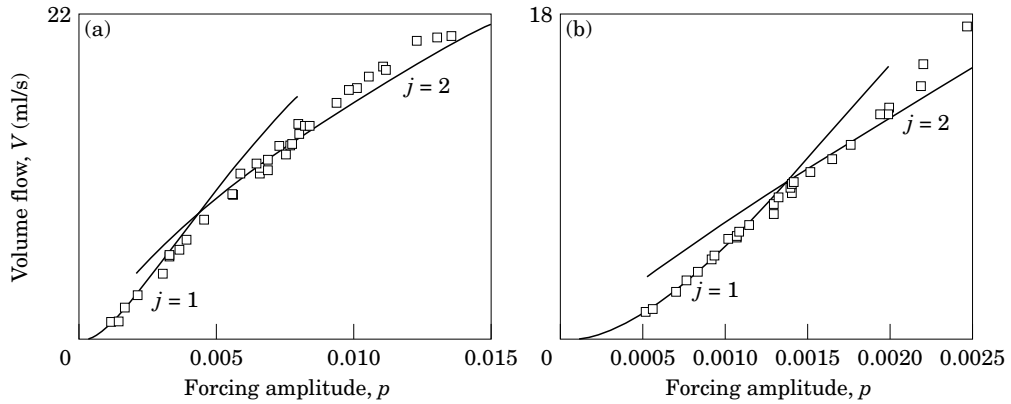

Figure 9. Experimental and theoretical values for the volume flow V (ml/s) versus the forcing amplitude p for the two lowest modes of vibration: ——, perturbation solution; □, experimental data; a) pipe 1, $\Omega = \omega_1$, $\alpha_1 = 0{\cdot}1$, $\alpha_2 = 2{\cdot}6$, $\zeta_1 = 0{\cdot}04$, $\beta^2 = 0{\cdot}39$; (b) pipe 2, $\Omega = \omega_2$, $\alpha_1 = 0{\cdot}22$, $\alpha_2 = 3{\cdot}9$, $\zeta_2 = 0{\cdot}03$, $\beta^2 = 0{\cdot}39$.

The results for both pipes show good agreement between predicted and measured volume flow. Maximum deviation is about 15%, but the bulk of the experimental points is seen to lie near the theoretical curves. Experimental results also seem to indicate the predicted shift from laminar flow ($j = 1$) to turbulent flow ($j = 2$), in that the location of the experimental points drops off to match the lower slope of the turbulent curves for higher values of p.

6. SUMMARY AND CONCLUSIONS

Vibration-induced fluid flow caused by nonlinear fluid-structure interaction has been investigated.

Equations of motion governing the transverse vibrations of a cantilever pipe and the speed of an internal incompressible fluid were derived. The two equations are coupled through nonlinear terms. The pipe vibrations affect the fluid through nonlinear forcing, and the induced fluid flow affects the vibrations of the pipe by modifying the damping and stiffness.

Numerical studies showed that the vibrations of the pipe cause the fluid to have a mean speed component towards the pipe end, in addition to a small oscillating component. Resonant excitation of all cantilever vibration modes can be used to obtain this effect. It was noticed that the magnitude of pipe vibrations necessary to obtain a given mean fluid speed is significantly lower for high modes.

A perturbation analysis was performed using a multiple-scales method. Frequency response curves were obtained for near-resonant excitation. Noticeable fluid motion occurs for near-resonant excitation only, where the nonlinear vibratory forcing is sufficiently large. The fluid damps the vibration amplitude in the resonant region. Two specific examples were considered: resonant excitation of the first and fourth modes of vibration. The results showed qualitative similarities. The response for the fourth mode of vibration is, however, affected by nonlinear pipe geometry, whereas for the fundamental mode this effect is negligible. The fluid damping effect on the pipe vibrations was seen to be largest for the fundamental mode, due to larger transfer of energy to the fluid.

The energy transfer mechanism in the system was analysed. It was shown that the efficiency factor, i.e. the kinetic energy of the fluid compared to the supplied energy by the vibration exciter, decreases with higher modes of vibration. The amount of viscous damping affects the efficiency of the system strongly, in that large dissipation decreases the energy transferred from the exciter to the fluid.

Experimental investigations were performed for resonant excitation of the first and second modes of vibration. The results showed good qualitative agreement with theoretical results for both laminar and turbulent flow.

This work has illustrated and quantified a phenomenon associated with nonlinear fluid-structure interaction. The nonlinear coupling explains transport of fluid through flexible cantilever pipes, as seen in experiments. Linear theory predicts no coupling between pipe- and fluid-motion and consequently no transport of fluid.

The phenomenon described, poses an alternative to previously suggested vibration conveyors, in that it relies on resonant excitation of an elastic structure. When resonant forcing is applied, fluid transport was shown to be possible for a wide range of system parameters. The efficiency associated with the fluid transport was shown to be rather low for realistic damping. There could, however, be other advantages using this device as a means of transporting/pumping. The mechanism is extremely simple with no internal moving parts. The device is therefore thought to be suitable for micro

purposes, e.g. applications in medicine. Advantages are also possible when dealing with toxic or aggressive fluids, which should not come into contact with moving parts.

Other means of excitation might also be used, e.g. parametric or transient excitation. Further work is required in these areas to understand this mechanism of transport fully. Also high-frequency excitation may introduce effects not included in the present model.

ACKNOWLEDGMENT

The author wishes to thank Jon Juel Thomsen for suggesting the project and for many valuable discussions

References

Babitsky, V. I. & Veprik, A. M. 1993 Damping of beam forced vibration by a moving washer. *Journal of Sound and Vibration* **166,** 77–85.

Bajaj, A. K., Sethna, P. R. & Lundgren, T. S. 1980 Hopf bifurkation phenomena in tubes carrying a fluid. *SIAM Journal of Applied Mathematics* **39,** 213–230.

Benjamin, T. B. 1961 Dynamics of a system of articulated pipes conveying fluid. I. Theory. *Proceedings of the Royal Society* (*London*) **A261,** 457–486.

Blekhman, I. I. 1994 *Vibrational Mechanics* (in Russian). Fizmatlit Publishing Company.

Blekhman, I. I. & Malakhova, O. Z. 1986 Quasiequilibrium positions of the Chekomei pendulum. *Soviet Physics Doklady* **31,** 229–231.

Chelomel, V. N. 1983 Mechanical paradoxes caused by vibrations. *Soviet Physics Doklady* **28,** 387–390.

Lee, U., Pak, C. H. & Hong, S. C. 1995 The dynamics of a piping system with internal unsteady flow. *Journal of Sound and Vibration* **180,** 297–311.

Long, Y. G., Nagaya, K. & Niwa, H. 1994 Vibration conveyance in spatial-curved tubes. *ASME Journal of Vibration and Acoustics* **116,** 38–46.

Nayfeh, A. H. & Mook, D. T. 1979 *Nonlinear Vibrations.* New York: Wiley-Interscience.

Païdoussis, M. P. & Issid, N. T. 1974 Dynamic stability of pipes conveying fluid. *Journal of Sound and Vibration* **33,** 267–294.

Païdoussis, M. P. & Li, G. X. 1993 Pipes conveying fluid: a model dynamical problem. *Journal of Fluids and Structures* **7,** 137–204.

Rousselet, J. & Herrmann, G. 1981 Dynamical behaviour of continuous cantilevered pipes conveying fluid near critical velocities. *Journal of Applied Mechanics* **48,** 943–947.

Sadiku, S. & Lepholz, H. H. E. 1987 On the dynamics of elastic systems with moving concentrated masses. *Ingenieur-Archiv* **57,** 223–242.

Semler, C., Li, G. X. & Païdoussis, M. P. 1994 The non-linear equations of motion of pipes conveying fluid. *Journal of Sound and Vibration* **169,** 577–599.

Thomsen, J. J. 1996 Vibration suppression using self-arranging mass: Effects of adding restoring force. *Journal of Sound and Vibration* **197,** 403–425.

White, F. M. 1991 *Viscous Fluid Flow.* New York: McGraw-Hill.

APPENDIX

The cantilever mode-shapes are given as:

$$\varphi_i(\xi) = \frac{\cosh \lambda_i + \cos \lambda_i}{\sinh \lambda_i + \sin \lambda_i}(\sin \lambda_i \xi - \sinh \lambda_i \xi) + (\cosh \lambda_i \xi - \cos \lambda_i \xi), \tag{A1}$$

where the $\lambda_i^2 = \omega_i$, $i = 1, \ldots, n$, are determined from the transcendental equations $\cos \lambda_i \cosh \lambda_i + 1 = 0$.

The first- and second- and fourth-order constants are defined as

$$\vartheta_i \equiv \int_0^1 \varphi_i \,\mathrm{d}\xi, \qquad h_{ik} \equiv -\int_0^1 \int_0^\xi \varphi_i' \varphi_k' \,\mathrm{d}\xi \,\mathrm{d}\xi,$$

$$k_{ik} \equiv \int_0^1 \varphi_i \varphi_k' \,\mathrm{d}\xi, \qquad g_{ik} \equiv \int_0^1 \varphi_i \varphi_k'' \,\mathrm{d}\xi, \qquad f_{ik} \equiv \int_0^1 \varphi_i \varphi_k''(1-\xi) \,\mathrm{d}\xi,$$

$$\Lambda_{iklm} \equiv \int_0^1 \varphi_i \varphi_k'''' \varphi_l' \varphi_m' \,\mathrm{d}\xi + 4\int_0^1 \varphi_i \varphi_k' \varphi_l'' \varphi_m''' \,\mathrm{d}\xi + \int_0^1 \varphi_i \varphi_k'' \varphi_l'' \varphi_m'' \,\mathrm{d}\xi,$$

$$G_{iklm} \equiv \int_0^1 \varphi_i \varphi_k'' \varphi_l' \varphi_m' \,\mathrm{d}\xi - \int_0^1 \varphi_i \varphi_k'' \int_\xi^1 \varphi_l' \varphi_m'' \mathrm{d}\xi \,\mathrm{d}\xi,$$

$$F_{iklm} \equiv 3\int_0^1 \varphi_i \varphi_k'' \varphi_l' \varphi_m'(1-\xi) \,\mathrm{d}\xi - \int_0^1 \varphi_i \varphi_k'' \int_\xi^1 \varphi_l' \varphi_m' \,\mathrm{d}\xi \,\mathrm{d}\xi,$$

$$H_{iklm} \equiv \int_0^1 \varphi_i' \varphi_k' \int_0^\xi \varphi_l' \varphi_m' \,\mathrm{d}\xi \,\mathrm{d}\xi,$$

$$\chi_{iklm} \equiv \int_0^1 \varphi_i \varphi_k' \int_0^\xi \varphi_l' \varphi_m' \,\mathrm{d}\xi \,\mathrm{d}\xi - \int_0^1 \varphi_i \varphi_k'' \int_\xi^1 \int_0^\xi \varphi_l' \varphi_m' \,\mathrm{d}\xi \,\mathrm{d}\xi \,\mathrm{d}\xi,$$

$$K_{iklm} \equiv \int_0^1 \varphi_i \varphi_k' \varphi_l' \varphi_m' \,\mathrm{d}\xi - \int_0^1 \varphi_i \varphi_k'' \int_\xi^1 \varphi_l' \varphi_m' \,\mathrm{d}\xi \,\mathrm{d}\xi.$$